ADVANCED SUSTAINABLE SYSTEMS
www.advsustainsys.com

Co-Assembly of Cellulose Nanocrystals and Silk Fibroin into Photonic Cholesteric Films

*Giulia Guidetti, Hui Sun, Alesja Ivanova, Benedetto Marelli, and Bruno Frka-Petesic**

Controlled self-assembly of bio-sourced nanocolloids is of high importance for the development of sustainable and low-cost functional materials but controlling nanocomposite fabrication with both satisfactory optical properties and composition remains challenging. Silk fibroin (SF) and cellulose nanocrystals (CNCs) have independently demonstrated their ability to produce high-quality photonic materials, in part due to their low absorbance and their transparency in the visible range. While SF is able to replicate inverse structures by high-resolution nano-templating, CNCs can spontaneously assemble into cholesteric liquid crystalline structures that are retained upon solvent evaporation, yielding photonic films. In this work, the conditions of successful co-assembly of regenerated SF, extracted from silkworm silk, with CNCs extracted from cotton, are investigated. Their co-assembly is investigated for various relative concentration ratios and pH, combining polarized optical microscopy and spectroscopy, SEM, and other characterization techniques (XRD, ATR-FTIR, TGA). The appearance of photonic properties is observed when CNC and SF are assembled at pH ≥ 4.15, highlighting the importance of suppressing attractive electrostatic interactions between the two species for an organized structure to emerge. Beyond its fundamental motivations for colloidal co-assembly with structural proteins, this work is relevant to design sustainable optical materials compatible with food packaging coatings and edible coloring pigments.

1. Introduction

The self-assembly ability of low-cost and bio-sourced colloidal particles into functional materials is an important branch of recent material science development, which is often expanded using various additives such as small molecules, polymers, proteins, or nanoparticles.[1] This addition often imposes a range of compatibility criteria that limits the type of additives that can be used, as well as the valid protocol conditions; however, these criteria are usually not well understood or poorly documented. If the conditions of compatibility for a successful one-pot co-assembly are not met, either no underlying order is preserved,[2,3] or the proposed preparation strategies have to circumvent the problem by introducing several additional steps relying on various post-treatments (e.g., swelling, infiltration, coatings, etc.).[4,5] While these alternatives are useful in many cases, their associated limitations justify investigating the conditions for successful co-assembly strategies in a much simpler one-pot approach.

Cellulose nanocrystals (CNCs) are one example of low-cost, bio-sourced, and renewable particles able to self-assemble into photonic films in presence of various additives, simply by drop-casting the suspension in a dish.[6–9] These chiral and splinter-like nanoparticles, isolated from cotton or wood pulp and recently at an industrial scale,[10–12] can spontaneously organize into a cholesteric liquid crystalline suspension above a threshold concentration.[13,14] Upon further solvent evaporation, the assembled structure gets kinetically arrested and further compresses vertically into a film displaying structural color.[15] Over the past two decades, many additional species have been investigated as additives to improve or propose innovative functionalities, for example, food-grade glitter,[6,16] mechanochromic response,[5,17,18] enhanced mechanical or adhesive properties,[19,20] exploration of possible chiral plasmonic effects,[21,22] or utilization as chiral templates for photonic mesoporous films,[23,24] to name a few. For these applications, successful co-assembly of CNCs has been observed with various types of species, including small molecules,[13,25] surfactants,[26] polymers,[19,20,27–30] or nanoparticles.[31–35] However, the cholesteric co-assembly of CNCs with structural proteins has been relatively unexplored.

Silk fibroin (SF) is a bio-sourced structural protein that can be extracted as a metastable suspension from *Bombyx mori* silk and further used as a highly versatile building block for a variety of applications.[36,37] This regenerated form of SF, obtained after the sericin gum has been removed, is both edible and injectable, easily processable and biodegradable, as well as able to resist large mechanical deformations, a property that is complementary to high Young modulus materials such as CNCs for the design of

Dr. G. Guidetti, Dr. A. Ivanova, Dr. B. Frka-Petesic
Department of Chemistry
University of Cambridge
Lensfield Road, Cambridge CB2 1EW, UK
E-mail: bf284@cam.ac.uk
Dr. G. Guidetti
Silklab
Department of Biomedical Engineering
Tufts University
200 Boston Avenue, Medford, MA 02155, USA
H. Sun, Prof. B. Marelli
Civil and Environmental Engineering
Massachusetts Institute of Technology
Cambridge, MA 02139, USA
The ORCID identification number(s) for the author(s) of this article can be found under https://doi.org/10.1002/adsu.202000272.

DOI: 10.1002/adsu.202000272

reinforced biocomposites and coatings.[38] The fibroin chains bear recurrent predominantly hydrophobic (Gly-Ser-Gly-Ala-Gly-Ala)$_n$ sequences, prone to fold into β-sheet structures through inter- and intra-molecular hydrophobic interactions and hydrogen bonding, and are interrupted by hydrophilic non-repetitive sequences.[39,40] SF has proved to easily self-assemble in solution into highly versatile structures, easily cast and molded into transparent and high quality optical and photonic components replicating features of few tens of nanometers.[41–44]

The association of SF and CNCs has been investigated to develop composite materials, focusing only on their enhanced mechanical properties, either as films,[45] or fibers,[46,47] without cholesteric structures and hence structural color. Freddi et al.,[48] and later several other groups,[49–52] reported SF-cellulose blend films made from dissolved and regenerated SF and regenerated cellulose (i.e., non-native cellulose II allomorph), with a general improvement of both strength and elongation at break or maintained optical transparency. In comparison, little work has been done using CNCs in their native form (cellulose I). The earlier report we found combining SF and cellulose I into composite films for mechanical reinforcement is from Noishiki et al. using CNCs,[53] later followed by other groups, using either CNCs,[47,54–57] or cellulose nanofibrils (CNFs).[57–61] In the work of Noishiki et al., *B. mori* SF was mixed at pH 7 to high aspect ratio CNCs extracted from tunicates, and reported an increase of the tensile strength by a factor ≈4 and of the ultimate strain by a factor ≈8 simply by incorporating 20 wt.% of SF in the composite. More recently, Cho et al. showed that SF films containing 1.5% of CNFs present an increase of their elongation at the break by +150% and of their Young modulus by +50%, while still maintaining a high transparency (i.e., 75% transmittance).[58] SF also presents an optical index (1.54) similar to the average optical index of CNCs films (1.555), which should benefit the optical properties of the composite.[62,63] All these results indicate that SF and CNCs can bind strongly to one another, which suggests this could also benefit the cohesion of composites in which the CNCs are self-assembled into a cholesteric order. Importantly, the demonstrated biodegradation of CNCs[64] and SF,[65] the food safe character of CNCs[66] and SF,[67] as well as the gas barrier function of densely packed CNCs films[68] and SF coatings,[38] make composite SF-CNC materials particularly interesting for the design of perishable food packaging.

In this work, we investigated the conditions required to successfully co-assemble SF and CNCs into photonic nanocomposite films, whereby a cholesteric order forms in suspension upon casting and is retained in the dry film, yielding structural color. The influence of the pH and the SF:CNC ratio are explored and related to the optical and structural characterization of the films, using polarized optical microscopy (POM) and scanning electron microscopy (SEM). Finally, the possible nature of the interactions between SF and CNCs is discussed in light of attenuated total reflection Fourier-transform infrared spectroscopy (ATR-FTIR) and thermal gravimetric analysis (TGA) characterizations.

2. Results

The results of this work are based mostly on one experimental dataset (SF-CNC-A) by default, while a second dataset (SF-CNC-B) is later introduced to complement the former, as described in the Experimental section and detailed in Table S1, Supporting Information.

2.1. Influence of pH on the Optical Properties

2.1.1. pH Adjustment in CNC Suspensions

Measuring the pH in acidic CNC suspensions appears to be non-trivial, as the value usually measured with a pH-probe is inconsistent with the titration of the same CNC suspension against the base. The pH probes usually require the suspension to be sufficiently conductive, but most of the cations present in the suspensions are not accompanied by an anionic counterpart to provide sufficient conductivity. Finally, leakage of KCl from the probe frit into the sample causes a drift of the pH values measured over time. This inconsistency is solved when a sufficient amount of KCl is added to the acidic CNC suspension (Figure S1, Supporting Information). For all these reasons, we adjusted the pH by titrating against NaOH and measuring the pH in sacrificial aliquots where dry KCl powder was added to it prior to the measurement. This gave stable and repetitive measurements of the actual content of H^+ ions in the CNC suspensions prior to SF addition, and these are the pH values reported throughout this work.

2.1.2. Visual Inspection of CNC and SF-CNC Films

First, films from CNC suspensions at pH 3.96 and pH 6.50 without any SF were cast as control samples and displayed comparable structural color (**Figure 1**a). The main significant difference between the two films is in the increased waviness of the films at higher pH, due to the progressive detachment of the films from the glass substrate upon drying. The samples prepared at lower pH appear systematically more attached to the glass, as a result of stronger attractive interactions between negative CNCs with the glass surface in an acidic environment.

The effect of progressive pH adjustment of the CNC suspension prior to the addition of SF was investigated by preparing films from suspensions mixed at SF:CNC ratio 10:90, with gradual pH increment from 3.96 to 6.50, as summarized in **Figure 2**b,c and Table S2, Supporting Information. Suspensions obtained by direct mixing at pH < 3.96 formed turbid suspensions and were not further investigated. Macroscopic photographs of the obtained films are reported in Figure 2a. The films produced at low pH displayed good transparency but no structural coloration (pH 3.96, SF:CNC 10:90). Instead, the films produced at higher pH co-assembled into a colored film (pH 6.50, SF:CNC 10:90), indicating that the cholesteric ordering of the CNCs was preserved. The structural color appeared above a pH threshold located between 3.96 and 4.15, while higher pH values did not drastically affect the hue by naked eye. Compared to pure CNC films, composite SF-CNC films were flat and well attached to the substrate, and their overall color appeared slightly red-shifted and more homogeneous than the pure CNC films

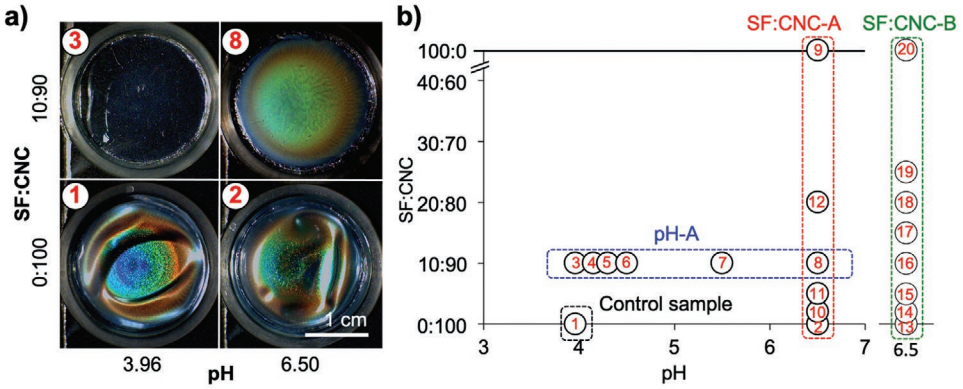

Figure 1. a) Macroscopic pictures of SF-CNC-A films cast at low pH (pH 3.96) and high pH (pH 6.50) for various SF:CNC ratios. b) Overview of the explored SF-CNC films casting conditions: (black dash) CNC-A film at low pH (control); (blue dash) pH-A series of composite SF-CNC-A samples at fixed SF:CNC ratio; (red dash) SF-CNC-A and (green dash) SF-CNC-B ratio series at constant pH 6.50. The numbers refer to the "# sample" in Table S2, Supporting Information.

cast in similar conditions. The samples also appear to have dramatically increased their interaction with the substrate: while the film cast at pH 3.96 could be easily peeled off, the film cast at pH 4.15 only partially detached, and all the other samples cast at higher pH were strongly attached to the glass substrate. Attempts to detach the films with a razor blade only led to scratches and the release of sub-millimeter particles, suggesting exceptionally good adhesion, possibly mediated by strong hydrogen bond interaction with -OH groups at the glass surface.

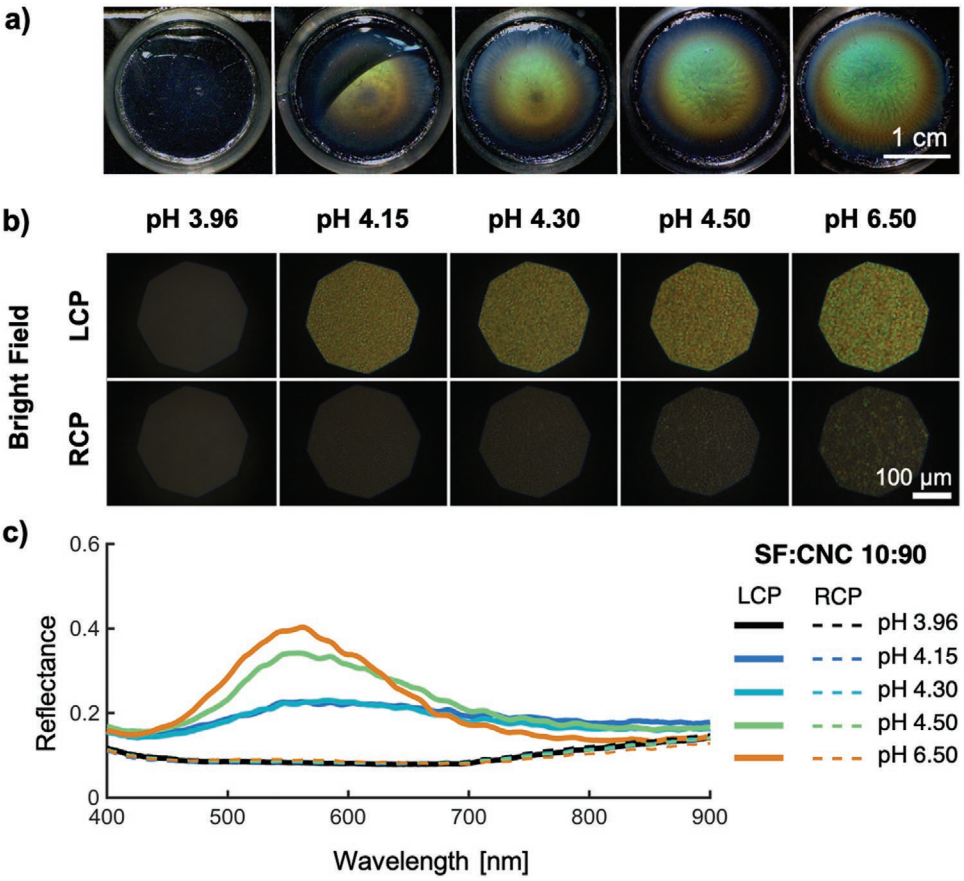

Figure 2. Optical properties of SF-CNC-A nanocomposites prepared from co-assembled SF and CNCs at volumetric ratio SF:CNC = 10:90 and increasing pH suspension (pH-A series). a) Macroscopic photographs of the films; b) POM in left- (resp. right-) circular polarization (i.e., LCP, resp. RCP) observed in BF; c) Corresponding reflectance spectra normalized to the LCP intensity reflected off a silver mirror.

2.1.3. Polarized Optical Microscopy

POM was used in reflection to investigate the local optical properties of the films. Observations in bright field (BF) with the selection of either left or right circularly polarized light components (i.e., LCP and RCP, resp.) are reported in Figure 2b. The films display an increasing reflectance in the LCP channel as the pH is increased, while the reflectance in the RCP channel remains low, as expected for a left-handed cholesteric structure. The mosaic-like pattern of the films indicates that they have a multi-domain structure. The domain boundaries appear more visible in the RCP channel and show an increase in their size with the pH (Figure S2 and Table S3, Supporting Information). Observations in dark field (DF) (Figure S3, Supporting Information) also display a similar trend (increasing signal in LCP compared to RCP), indicating that the multi-domain cholesteric structure is due to distinct orientation between domains, as their misalignment from the normal direction induces reflection at broader angles.[69]

2.1.4. Reflectance Spectra in POM

The reflectance spectra of the films were analyzed by collecting separately the LCP and RCP light, as reported in Figure 2c. The evolution of the LCP reflectance peak upon pH increase shows initially a sharp transition, from no peak at all at pH 3.96, to a peak at pH 4.15. As the pH increases further, the reflected peak develops, and the reflected peak slightly blueshifts to reach 560 nm. The reflectance in RCP shows no peak for all the samples, as expected from a left-handed cholesteric structure at normal incidence.[15]

2.2. Influence of SF:CNC Ratio on the Optical Properties

The effect of the SF:CNC ratio has been investigated by fixing the NaCl:CNC ratio, which means that the absolute concentration of NaCl was adjusted to a smaller value in a suspension with a smaller CNC fraction (and higher SF fraction). This was motivated by the fact that in pure CNC films, the NaCl:CNC ratio directly impacts the film color, causing blue-shifts at a higher NaCl:CNC ratio. The exact composition of the suspensions used to prepare all the films is detailed in Table S2, Supporting Information.

2.2.1. Visual Inspection of the SF-CNC Films

Macroscopic photographs of the obtained films, reported in **Figure 3**a, reveal the effect of progressive increase of volumetric SF:CNC ratio at fixed pH 6.50. At that pH, the structural color is preserved for all investigated ratios, while pure SF film gives a highly transparent film with no structural color. The color appears gradually red-shifted as the SF:CNC ratio increases, and the color homogeneity across the sample is also improved.

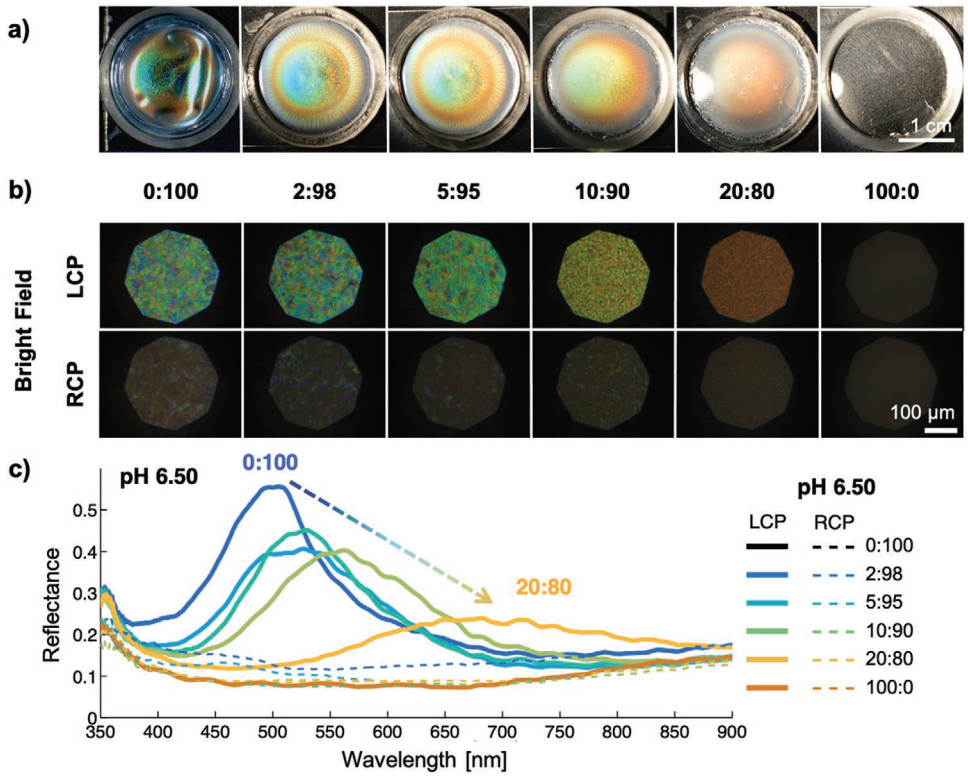

Figure 3. Optical properties of SF-CNC-A nanocomposites prepared at pH 6.50 and increasing SF:CNC ratio: a) macroscopic photographs of the films; b) POM observed through LCP and RCP filters, respectively; c) Corresponding reflectance spectra, normalized to the LCP intensity reflected off a silver mirror. The introduction of SF induces a red-shift and a broadening of the reflected peak.

2.2.2. Polarized Optical Microscopy

The films were analyzed with POM in BF in both LCP and RCP channels, as reported in Figure 3b. The films display a strong reflectance in the LCP channel that progressively red-shifts as the SF:CNC ratio increases, while the reflectance in the RCP channel remains low, except in few locations. The mosaic-like pattern indicative of a multi-domain structure is also observed, and observations in the RCP channel show a clear decrease of their size as the SF:CNC increases (Figure S4 and Table S4, Supporting Information). This trend is confirmed by observations in DF (Figure S5, Supporting Information) displaying a speckly appearance with a coarser aspect at low SF:CNC ratios.

2.2.3. Reflectance Spectra in POM

The reflectance spectra of this sample series have been systematically analyzed on areas of ≈700 μm^2 as shown in Figure 3c. A clear red-shift of the reflected peak is confirmed in the LCP channel, together with a broadening of the reflectance peak and a decrease of its intensity, while the RCP reflectance remains low (NB: the increasing baseline above 700 nm is an artifact from the substrate). The observed red-shift is expected when introducing a non-volatile co-solvent, provided it does not interfere much with the CNC self-assembly, as it has been already reported for polyethylene glycol, glycerol, and glucose.[6,19,25] It can be explained as following: in the final drying steps, the assembled structure undergoes a gelation transition that locks the arrangement of its colloidal species, and the further evaporation of the remaining water compresses the structure vertically into a dry solidified film.[69–71] The presence of a non-volatile co-solvent thus prevents the full shrinkage of the final cholesteric structure upon drying and therefore leads to a larger cholesteric pitch. The broadening of the peaks can be understood as a consequence of the increasingly more polydomain structure of the film as more SF is present, increasing light scattering but also the misalignment of the domains, causing spreading of the local pitch values.[69]

2.3. Structural Analysis of the Films

The internal structure of the films was investigated by imaging their cross-section by SEM, as illustrated in **Figure 4** and Figure S6, Supporting Information. First, the SEM of the film prepared without any SF (SF:CNC 0:100, pH 6.50) presents crack patterns with clear Bouligand arches at high magnification,[72,73] while the low magnification image is characteristic of a polydomain cholesteric structure (Figure 4a). In contrast, the film prepared with SF added at low pH (SF:CNC 10:90, pH 3.96) displays at low magnification a uniform smooth interface of its cross-section, with no clear evidence of a cholesteric order at high magnification (Figure 4b). We note that a periodicity under 100 nm can be distinguished on this image, but it is difficult to interpret and too small to produce any photonic response in the visible range. The smooth crack profile implies that the crack propagated easily and that the surface area of the crack propagation remained low as in a more brittle material. Finally, the cross-section of the sample prepared with SF at higher pH

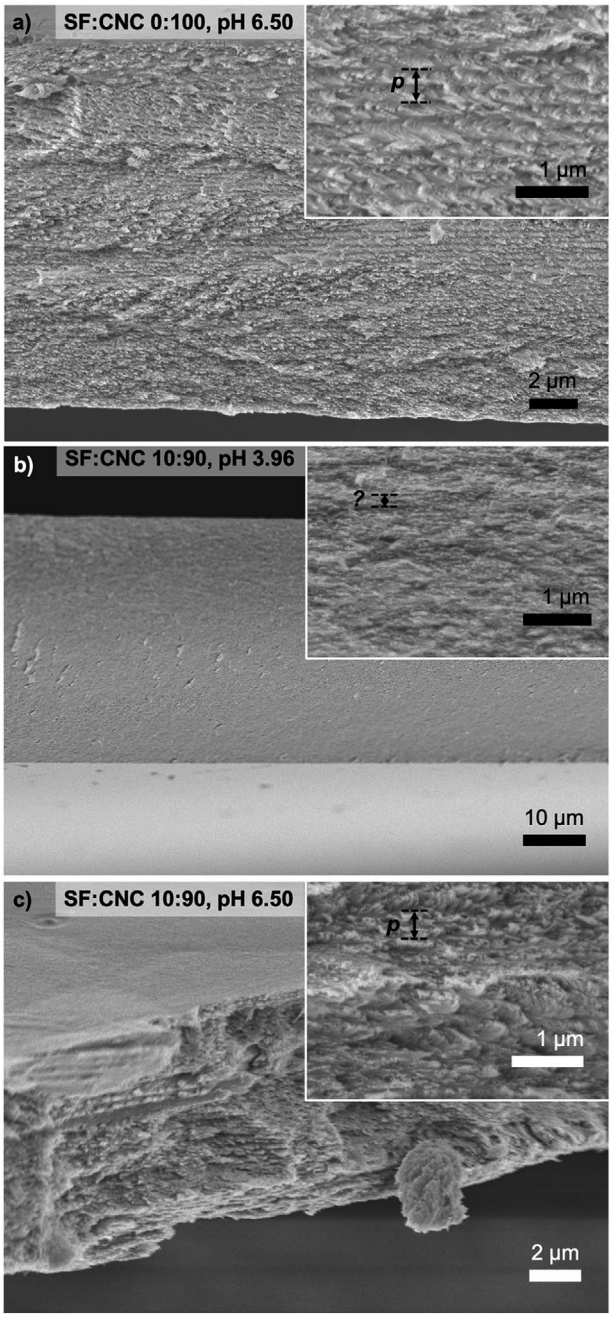

Figure 4. SEM images of film cross-sections: a) pure CNC-A films (SF:CNC 0:100, pH 6.50); b) SF-CNC-A composites (SF:CNC 10:90, pH 3.96); c) SF-CNC-A composites (SF:CNC 10:90, pH 6.50). Corresponding high magnification SEM images are shown in insets.

(SF:CNC 10:90, pH 6.50) appears with visible chiral arches at high magnification, confirming the preservation of the cholesteric order in the composite (Figure 4c). Interestingly, the cross-section of the composite appears much more irregular than in the SF:CNC 0:100 pH 6.50. This correlates with a smaller domain size observed in POM and suggests that the more tortuous crack propagation is influenced by the irregular mechanical properties between cholesteric domains at the domain boundaries.

2.4. Silk Fibroin Conformation

The conformation of SF can have a strong influence on its mechanical properties but also on the nature of the interactions between SF and CNCs.[74] They have been investigated by combining X-ray diffraction (XRD), ATR-FTIR, and TGA.

2.4.1. X-Ray Diffraction Analysis

XRD spectra have been recorded on films cast at pH 6.50 and at SF:CNC ratios of 0:100 (pure CNC), 10:90, and 100:0 (pure SF), as shown in Figure S7, Supporting Information. In the two samples containing CNCs, three peaks at $2\theta = 14.76°$ ($1\bar{1}0$), 16.44° (110), and 22.56° (200) confirmed that native cellulose (cellulose I) was maintained after the acid hydrolysis preparation and pH adjustment, as well as in co-assembly with SF.[75–77] The XRD pattern of the pure SF sample presented the main peak at 2θ = 21.4° indicating rather a hydrophilic, helix-rich conformation also found in silk I.[78] However, the CNC signal in the composite film dominated the one from the SF and thus could not lead to a reliable determination of the SF conformation inside composites using this technique.

2.4.2. ATR-FTIR Analysis

ATR-FTIR spectroscopy analysis was carried out on the films and reported in **Figure 5** and Figure S8, Supporting Information. We first discuss the absorption band attribution and their relevance to SF-CNC composites, and then the effects of pH and SF:CNC ratio on the SF conformation.

Band Attribution: To determine the conformational structure of the fibroin films in the composites, the amide I region between 1600 and 1700 cm^{-1} is the most reliable and corresponds to the C=O stretching mode. The amide II region, between 1555 and 1515 cm^{-1}, is rarely used as the N−H bend can be influenced by other factors. Finally, the amide III region (C−N stretching, 1230–1270 cm^{-1}) overlaps with cellulose signal (COH bend at C6, 1235 cm^{-1}; C−C, C−O, and C=O stretch, 1250 cm^{-1}) and is ignored in this work.[79,80]

Conformations characteristics of soluble silk (such as mostly found in silk I) are associated with bands between 1638–1646 cm^{-1} (random coils, extended chains), 1647–1655 cm^{-1} (random coils), and 1656–1662 cm^{-1} (alpha helices) in the Amide I region,[81] and between 1535–1555 cm^{-1} in the Amide II region.[82,83] In contrast, the insoluble conformations (as found mostly in silk II) are found between 1616–1621 cm^{-1} (aggregate β-strand, β-sheets, weak signal), 1622–1637 cm^{-1} (β-sheets, strong signal), and 1697–1703 cm^{-1} (antiparallel β-pleated sheets, weak signal) in the Amide I region,[81] and between 1516–1530 cm^{-1} in the Amide II region.[82] For clarity, these regions are highlighted in light red (soluble conformations) and light blue (insoluble conformations) bands in Figure 5.

Moreover, the restriction to the analysis of the amide I region has proven to give a reliable evaluation of the proportion of the different local conformations of silk such as random coils, helices, β-sheets, and turns.[84] Note that pure CNCs present a small and broad band around 1631 cm^{-1} ascribed to the -OH bending mode of the absorbed water which can slightly interfere with the amide I bands, while it has no signal in the amide II region.

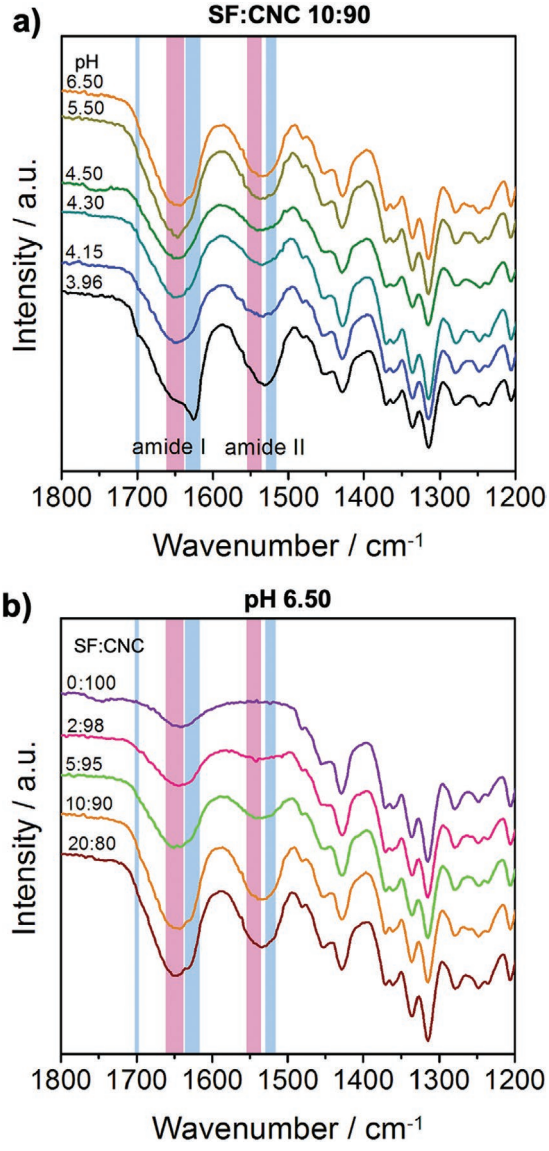

Figure 5. ATR-FTIR spectra of SF-CNC-A nanocomposites films obtained by casting suspension a) at SF:CNC ratio 10:90 and increasing pH; b) at pH 6.50 and increasing SF:CNC ratio. Vertical bands highlight the contributions ascribed to soluble conformations (red) and insoluble (blue) conformations. In both graphs, the orange line corresponds to the same sample (SF:CNC 10:90, pH 6.5).

SF Conformation Versus pH: The effect of pH is illustrated in Figure 5a, where the spectra of SF-CNC-A samples prepared at fixed volumetric ratio SF:CNC 10:90 and increasing pH are compared. The peak broadness indicates a rather statistical mixture of these secondary structures, with, however, some clear tendencies. At any pH ≥ 4.15 (i.e., in all colored composite films), the amide I region is dominated by a broad peak in the range 1640–1660 cm^{-1} and the amide II band is centered around

1538 cm^{-1}, both indicating predominant soluble conformations. However, for pH 3.96 (i.e., in a film showing no structural color and no apparent cholesteric order in cross-sectional SEM), a strong additional band is present at 1625–1632 cm^{-1}, while the amide II band is shifted to lower wavenumbers, which clearly indicates a SF structure with more insoluble conformations. A small shoulder is observed at 1700 cm^{-1}, which is characteristic of antiparallel intermolecular β-sheets.

This strongly suggests that soluble silk conformations are associated with successful self-assembly at pH ≥ 4.15, while the presence of insoluble silk conformations correlate with an unsuccessful CNC self-assembly and a loss of the photonic properties.

SF Conformation Versus SF:CNC Ratio: The effect of the SF:CNC ratio is illustrated in Figure 5b, where the spectra between SF-CNC-A samples prepared at fixed pH 6.50 and increasing volumetric SF:CNC ratio are compared. In this series, all composite SF-CNC conformations are dominated by soluble secondary structures, as expected in films obtained by simply casting SF in ambient conditions. However, a shoulder characteristic of β-sheet structures remains noticeable at 1625 cm^{-1} and gets stronger as more SF is added. This suggests that part of the SF always adopts a β-sheet structure when getting in close contact with CNCs. To assess this possibility, an aqueous SF solution was also analyzed (Figure S8a, Supporting Information) and showed no signal in this region. However, a film made only from SF (SF:CNC 100:0 pH 7) and that aged for several months was also analyzed for comparison (Figure S8a, Supporting Information) and also showed a small conformational change around 1625 cm^{-1}. The signal at 1625 cm^{-1} being weak in both cases, it is most likely that these insoluble SF conformations occurred after the self-assembly took place but that they were not present when the two species interacted in suspension.

Methanol Vapor Treatment: From the observations reported so far, structurally colored SF-CNC films contained mostly soluble silk conformations, while insoluble conformations such as β-sheets are usually more desirable for better material cohesion. A transition from helix to β-sheet structures is commonly achievable with annealing treatments such as, for example, methanol vapor, UV radiation, heat treatment at higher humidity, or stretching. To investigate this possibility, we characterized the ATR-FTIR spectra of a film (SF:CNC 20:80, pH 6.50) before and after applying a methanol vapor treatment. After methanol treatment, a dominant peak appeared between 1632 and 1625 cm^{-1}, indicating that it is still possible to adjust at will the final SF structure in the SF-CNC composites without affecting the optical response (Figure S8b, Supporting Information).

2.4.3. Thermal Stability

The thermal stability of SF-CNC films can offer complementary information to the local nanostructure in the composite. This was analyzed by TGA and compared to pure CNC and SF films, all cast at pH 6.50, as shown in Figure S9, Supporting Information. The pure CNC film presents a main sharp degradation peak around 220 °C and a smaller one around 305 °C in derivative thermal gravimetric analysis (DTGA) (Figure S9b, Supporting Information), while pure SF shows a broader degradation around 280–320 °C. Around 700 °C, both have degraded with a comparable residual mass about 30% of the initial mass, which facilitates the comparison between the samples. The composite SF:CNC 10:90 presents two different peaks in DTGA. These peaks are similar to those observed in pure CNC films but shifted to higher values, namely 250 and 350 °C. Note that the mass fraction of SF in this sample is 9%, and accordingly, only a small contribution of SF mass loss is expected and probably contributes to the signal between the two peaks, at 300 °C. Such an increase in the degradation temperature indicates that, in spite of its small mass proportion, SF significantly increases the thermal stability of the CNC fraction in the composite. We postulate that this thermal stability originates from the reduced permeability of the composite and partial adsorption of the SF onto the CNC surface.

2.5. Optimization of SF-CNC Films

The results presented so far are all based on the dataset of SF-CNC-A films, which were cast in small custom-made dishes that led to significant edge effects. Building on the acquired know-how, we prepared a second series of films with different batches of SF and CNC suspensions with similar properties (SF-CNC-B), cast in glass Petri dishes (Table S1, Supporting Information, films #1) with various SF:CNC ratios at pH 6.5. The obtained series is presented in **Figure 6** and shows well-adsorbed films with a uniform structural color. While the only noticeable difference in the two protocols is the ratio of electrolyte to CNC (ca. 100 μmol g^{-1} in SF-CNC-B series instead of ca. 200 μmol g^{-1} as in the SF-CNC-A series), the films show essentially the same trend, namely a successful co-assembly of SF and CNCs, with a red-shift of the color with respect to the SF:CNC ratio, and a strong adhesion onto the Petri dish in presence of SF even for SF:CNC 2:98.

2.6. Tensile Test of SF-CNC Films

The mechanical properties of the SF-CNC films were estimated using a tensile test on free-standing composite films. These films were prepared by casting the optimized SF-CNC-B suspension with various SF:CNC ratios at pH 6.5, on a superhydrophobic substrate within wetting rings simply placed on it (Table S1, Supporting Information, films #2). The tensile test allowed us to estimate the Young modulus and the ultimate tensile strength of the films, as reported in Figure S10, Supporting Information. The Young moduli of the composites were slightly improved (by a fact or of ≈2 at best) when compared to the films made entirely from SF or from CNCs. The ultimate tensile strength appeared to decline more significantly as more SF is added, suggesting SF acts as a plasticizer. The films appeared bendy and could fold back but also break easily upon tension. Overall, the poor reinforcing effect of incorporating SF in structurally colored CNC films may result from the very same conditions of weak interactions between SF and CNCs required to yield the formation of a cholesteric order. These films, cast at

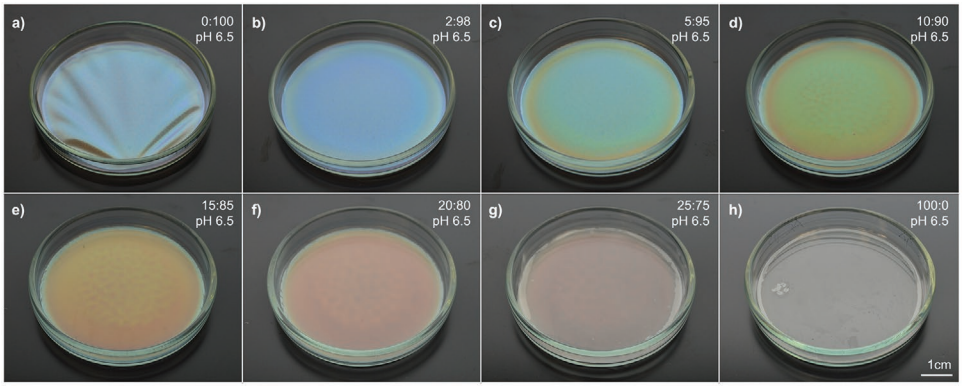

Figure 6. Macroscopic photographs of SF-CNC-B nanocomposites films obtained by casting at half the NaCl:CNC ratio used in SF-CNC-A (ca. 100 μmol g^{-1} instead of ca. 200 μmol g^{-1}). SF:CNC ratios are as it follows: a) 0:100, b) 2:98, c) 5:95, d) 10:90, e) 15:85, f) 20:80, g) 25:75, and h) 100:0.

pH 6.5, may thus display a reduced cohesion between its constituting components. In contrast, a clear mechanical reinforcement in SF-CNC composites was observed by Noishiki et al., but without any cholesteric order and with CNCs extracted from tunicates.[53] It is possible that their much bigger aspect ratio (with CNCs over one micrometer long) accounted for a better synergetic reinforcement effect between SF and CNCs. Further work is required to validate this scenario.

3. Discussion

3.1. Comparison of Native SF with Regenerated SF

The self-assembly of CNCs into a cholesteric suspension is observed above a critical pH located between 3.96 and 4.15. This pH can be compared to the isoelectric point (pI) of the SF, which actually contains several compounds.

3.1.1. Composition of Native SF In Vivo

Native SF, as found in vivo in *B. mori,* is made of three compounds, namely a heavy chain (350 kDa), a light chain (26 kDa), and a glycoprotein P25 (about 30 kDa) in a 6:6:1 molar ratio.[85] The isoelectric points of each of these compounds are, respectively, 4.39, 5.06, and 6.69.[86] The specific pI of the hydrophilic N-terminal and the C-terminal of the heavy chain are 4.59 and 10.53, respectively, while the hydrophilic spacers that lie between the hydrophobic blocks in the central domains of silk proteins have a pI estimated to 4.03 for *B. mori*, with a charge distribution that is rather consistent along the length of the molecule.[86] At pH lower than 10.53, the C-terminal end of the H-chain is positively charged and is linked to the negatively charged L-chain by an intermolecular S—S disulfide bond between two cysteines. As the size of the L-chain is about 5 times larger than the C-terminal group, the local charge of the complex is expected to be mostly negative above the pI of the L-chain, namely pH ≥ 5.06. This complex is then believed to associate with P25 through non-covalent hydrophobic interactions in the molar ratio of 6:6:1 to form a quaternary protein complex known as an elementary unit.

The silk glands of the *B. mori* produce SF as an aqueous solution rich in random coils and helices (silk I) and the gradual decrease of the pH from the posterior divisions of the gland (pH 6.9) till the anterior division (pH 4.8) is believed to trigger the precipitation of native SF into silk II fibers, where insoluble β-sheets are predominant. Specific ions are also believed to play an important role in this folding process: Na^+ and Cl^- ions in the posterior divisions of the glands are progressively swapped by chaotropic ions such as K^+ and Ca^{2+} in the anterior divisions prior to extrusion (from ≈5 to ≈15 mM), as they increase the solubility of hydrophobic regions and favor transient unfolding required to create inter-molecular β-sheet-rich hydrophobic bonds.

3.1.2. Composition of Regenerated SF

The composition of regenerated SF is greatly affected by the regeneration process.[87] During degumming (i.e., removal of the sericin glycoprotein), SF was exposed to alkaline pH and $T > 100$ °C, which is known to cause a lot of damage to all three chains. P25 is likely broken down and is then dialyzed out during dialysis. The heavy and the light chains are also broken into smaller components, yielding a mix of smaller proteins with a molecular range between 350 Da and 10 kDa. For these reasons, the pI of this regenerated SF is expected to be around 4.5 on average, although it can vary with the sample preparation from 3.9 to 4.8.

Once combined with CNCs, the SF suspension is also in a different physical environment, even without directly interacting with the CNCs. The ionic content is limited to low concentration of kosmotropic ions ($[Na^+] \leq 8$ mM, $[Cl^-] \leq 4$ mM) and the absence of K^+ and Ca^{2+}, overall limiting the exposition of hydrophobic regions. Also, in contrast with native silk upon extrusion, no shear is applied during the self-assembly process.

3.2. Criteria for SF-CNC Co-Assembly into Cholesteric Structures

Maintaining a successful co-assembly of SF and CNCs into a cholesteric structure requires the prevention of strong complexation between SF and CNCs. An unsuccessful co-assembly

observed at pH ≤ 4, as well as an already good co-assembly at pH ≈ pI = 4.5, suggests that the co-assembly is prevented when the SF chains have developed a sufficiently large positive net charge, causing their collapse onto negatively charged CNCs (bearing $-OSO_3^-$ groups) and even bridging them together. CNCs also present −OH surface groups that favor insoluble silk structures via hydrogen bonding with amide −NH groups.

In contrast, films prepared at higher pH prevented this complexation and maintained the ability of CNCs to self-assemble into a cholesteric structure. However, POM and SEM observations indicate that samples prepared at intermediate pH values displayed a much more pronounced polydomain structure. We speculate that in these samples, part of the SF has adsorbed onto CNCs and caused local aggregation, contributing to the development of the domain boundaries observed under POM.

3.3. Effect of Geometry and NaCl:CNC Ratio

The optical appearance of SF-CNC films can be optimized by casting suspension on larger surfaces (e.g., in larger glass Petri dishes) in order to minimize the edge effect and benefit from the adherence of the films to the substrate. Moreover, the NaCl:CNC ratio can be varied to adjust the optical response to fit the needs of a different CNC batch, without much consequences on the SF and the SF-CNC co-assembly.

4. Conclusions

The conditions leading to successful co-assembly of SF and CNCs into ordered chiral photonic structures were investigated. When the SF solution is added to a CNC suspension at low pH (pH ≤ 4.1 ± 0.1), the cholesteric co-assembly is disrupted and insoluble silk conformation with the typical β-sheet structure is found. In contrast, increasing the pH ≥ 4.15 allows for the cholesteric co-assembly of SF and CNC, with silk conformation indicative of a dominant disordered random coil structure. A post-treatment with methanol vapor was shown effective to convert the silk conformation to a dominant β-sheet structure, which can be exploited to adjust the cohesion of the composite. As the pH is increased up to pH 6.5, an improvement of the co-assembly at a larger length scale is clearly observed, resulting in larger cholesteric domains and stronger optical response. The origin of this co-assembly transition is ascribed to an electrostatic complexation occurring at lower pH between negatively charged CNCs and positively charged SF chains, a condition met at pH sufficiently lower than the pI = 4.5 of SF. At higher pH, the reflected color of the composite is red-shifted and decreases in intensity as more SF is added. The SF:CNC films were strongly attached to the glass substrate compared to the pure CNC films, suggesting strong hydrogen bond mediated interactions with −OH groups from the glass surface.

Structurally-colored SF-CNC films are fully biocompatible optical materials that can find applications as non-bleaching food-grade "effect" pigment,[16] colorimetric optically-responsive films,[88] or UV-light screening agents.[89,90] Moreover, the SF and CNCs combination to form structurally-colored composites involves no chemical reaction, and therefore is expected to retain the biodegradable, food-safe, and gas barrier properties of both SF and CNCs.[38,64–68] This indicates that SF-CNC films can be particularly promising for the design of fully biosourced, renewable, and biodegradable optical materials compatible with food packaging and edible coloring coatings. More generally, this work should also open opportunities to investigate further the ordered co-assembly processes of CNCs with other structural proteins, surface adhesion of films, and dispersion casting for the design of sustainable optical materials.

5. Experimental Section

Cellulose Nanocrystal Suspensions: Two comparable suspensions, referred to as CNC-A and CNC-B, were used in this work. Unless otherwise stated, the CNC-A was used as default. Both CNC suspensions were obtained from the hydrolysis of Whatman No. 1 cellulose filter paper (60 g) with sulfuric acid (64 wt.%, 840 mL) for 30 min at either 66 °C (CNC-A) or 60 °C (CNC-B), before being quenched using Milli-Q ice and water.[69,70] Soluble cellulose residues and acid were removed by centrifugation (three steps at 20 000 g for 20 min) and dialysis against deionized water (MWCO 12–14 kDa membrane). The detailed description of the suspension preparation and characterization are described in Table S1, Supporting Information. Conductivity titration against sodium hydroxide indicated $[H^+] = [-OSO_3^-] = 221$ µmol g^{-1} (CNC-A) or 227 µmol g^{-1} (CNC-B) on CNC surface (Figure S11, Supporting Information). The suspension was tip-sonicated in an ice bath (Fisherbrand Ultrasonic disintegrator 500 W, amplitude 30% max), vacuum-filtered (8.0 µm then 0.8 µm nitrocellulose, Sigma-Aldrich). CNC-A was additionally treated with mixed-bed ion exchange resin (Dowex Marathon MR-3), which was first thoroughly rinsed in Milli-Q water and then added to the CNC suspension for few days, then removed through filtration (8.0 µm nitrocellulose). Conductometric titration revealed no significant change before (221 µmol g^{-1}) and after (222 µmol g^{-1}) this additional treatment. The CNC-A after this treatment (2.32 wt.%.) and the CNC-B were both used to prepare SF-CNC composite films, as detailed in Tables S1 and S2, Supporting Information. Both CNC suspensions have only H^+ as counter-ions (acidic form) prior to pH adjustment.

Regenerated Silk Fibroin: Two suspensions of regenerated silkworm SF were used in this work, SF-A and SF-B, which were prepared following the same protocol.[91] Unless otherwise stated, SF-A was used as default. Cocoons from *B. mori* silkworms were boiled for 30 min in an alkaline solution of 20 mM Na_2CO_3 to remove the sericin glycoprotein. The extracted fibroin was rinsed with distilled water and then dried in ambient air for 12 h. After drying, the fibroin was dissolved in a 9.3 M LiBr solution at 60 °C for 4 h, yielding a 20 wt.% aqueous solution. Subsequently, the solution was dialyzed against distilled water using a dialysis cassette (Slide-a-Lyzer, Pierce, MWCO 3.5K) at room temperature for 48 h until the solution reached a concentration of 7 wt.%. The obtained solution was purified using a centrifuge and a 0.8 mm syringe filter.

Film Preparation: The CNC suspensions were diluted with Milli-Q water and NaOH 0.1 M to adjust to the aimed pH, therefore replacing progressively the H^+ counter-ions by Na^+. The pH was controlled with a pH-meter (pH probe Inlab Micro Pro, Mettler Toledo) in sacrificial aliquots of ≈0.2 mL where a few µg of dry KCl (Sigma Aldrich, 99.99%) were added prior to measurement to allow for a stable pH reading. The SF-CNC suspensions were prepared by two slightly different methods. In SF-CNC-A, NaCl 0.1 M was added to the pH-adjusted CNC-A, then SF-A, and finally Milli-Q water were added to adjust for the aimed volumetric ratio of SF:CNC (assuming a density of 1.4 and 1.6 g cm^{-3} for SF and CNCs, respectively) but also the [NaCl]/[CNC] ratio and the concentration [CNC]. In SF-CNC-B, pH-adjusted CNC-B suspensions were first diluted with milli-Q, then SF-B was added, and finally NaCl 0.02 M, aiming for a smaller ratio of [NaCl]/[CNC]. At this concentration,

the gradual pH neutralization of the CNC counter-ions with NaOH is responsible for additional $[Na^+] \approx 10^{-2.3} - 10^{-pH} \approx 4$ mM above pH 4. The mixtures were gently mixed with a micropipette immediately after preparation to avoid the introduction of bubbles. The films were cast by two different methods. SF-CNC-A was cast by placing 1.5 mL of the corresponding suspension into a custom-made dish, consisting of an acrylic ring (inner diameter 21 mm) glued onto a pristine microscope glass slide (cyanoacrylate-based glue) and left to dry in ambient conditions (T ≈ 23 °C, RH ≈ 30%). SF-CNC-B films were cast by placing 5.2 mL of the corresponding suspensions into a glass Petri dish (inner diameter 6.2 mm). All the suspensions were left to dry in ambient conditions (T ≈ 23 °C, RH ≈ 30%).

Optical Characterization: Macroscopic photographs were taken in two different configurations. For SF-CNC-A, the samples were placed above a localized source of light and the camera was oriented with an angle ≈10° from the normal of the films. For SF-CNC-B, the samples were placed in front of a diffuse source of light and the camera was oriented with an angle ≈38° from the normal of the films. Optical microscopy characterization was performed in reflection mode on a customized Zeiss (Axio Scope.A1 Vario) microscope using a halogen lamp (Zeiss HAL100) as a light source using Koehler illumination. Samples were observed with Zeiss Epiplan Apochromat objectives (5×, 10×, 20×) both in BF and DF. The light reflected off the sample was directed through a quarter-wave plate and a polarizing filter, specifically oriented to select either left-circularly-polarized (LCP) or right-circularly-polarized (RCP) light before being split between a CCD camera (UI-3580LE-C-HQ, IDS) and an optical fiber (600 µm—conjugated spot diameter 15 µm for a 20× objective) mounted in confocal configuration and connected to a spectrometer (AvaSpec-HS2048, Avantes). This setup allowed for the spectra acquisition from specific areas in the sample, in both polarization channels; all the spectra were normalized to the reflection of a silver mirror in the LCP polarization channel.

Scanning Electron Microscopy: SEM images were acquired using a Leo Gemini 1530VP system, Zeiss, working in cross-section at an angle of 90° with respect to the electron beam. The films were detached and cracked to image their cross-section. The produced flakes were placed on aluminum stubs using conductive carbon tape and sputter-coated with a 5–10 nanometer thick layer of Au/Pd (Emitech K550; I = 55 mA for 10–14 s) to minimize the charging effect. The acceleration voltage used was 5 kV and the working distance was 3–4 mm.

Composite Characterization: ATR-FTIR spectra were recorded on detached free-standing film flakes with a Perkin Elmer 100 FT-IR spectrometer, with a resolution of 4 cm^{-1} and accumulation of 4 scans between 4000 and 650 cm^{-1}. The XRD spectra were acquired with a PANalytical X-ray diffractometer operating with a Cu Kα radiation source (λ = 1.5405 Å) and recorded in the 2θ range of 5 to 60 degrees for 25 min. TGA was performed on a TGA/DSC2 STARe System Mettler Toledo with a heating rate of 10 K min^{-1} in nitrogen gas at a 100 mL min^{-1} flow rate.

Tensile Tests: Tensile tests were performed on a tensile Hounsfield machine equipped with a 5 N load cell, at a specific deformation rate (1 mm min^{-1}). The films were cut with a razor blade into strips with dimensions ca. 50 mm (L) × 5 mm (W) × 0.03 mm (T). The W and T dimensions were determined using, respectively, a caliper and an optical microscope, while the effective length between the clamps (L_{eff}) was measured with a caliper (≈20 mm). The films were glued onto a cardboard frame to facilitate positioning and to prevent slip in the clamps. The tested composite samples were free-standing films obtained from the series "SF-CNC-B films #2" but the SF-CNC 0:100 film was taken from the series "SF-CNC-B films #1" as it was already free-standing.

Supporting Information

Supporting Information is available from the Wiley Online Library or from the author.

Acknowledgements

The authors thank Silvia Vignolini and Fiorenzo G. Omenetto for fruitful discussions. This work was supported by the EPSRC (award 1525292) to G.G., the MSCA Individual Fellowship (award BINGO 743543) to A.I., the Office of Naval Research, USA (award N000141812258) and the National Science Foundation, USA (award CMMI-1752172) to BM.

Conflict of Interest

The authors declare no conflict of interest.

Data Availability Statement

The data that support the findings of this study are openly available from the University of Cambridge data repository (http://doi.org/10.17863/CAM.65066).

Keywords

cellulose nanocrystals, cholesteric, co-assembly, colloidal liquid crystals, silk fibroin, structural colors

Received: November 30, 2020
Revised: March 16, 2021
Published online:

[1] M. A. Boles, M. Engel, D. V. Talapin, *Chem. Rev.* **2016**, *116*, 11220.
[2] R. Xiong, H. S. Kim, S. Zhang, S. Kim, V. F. Korolovych, R. Ma, Y. G. Yingling, C. Lu, V. V. Tsukruk, *ACS Nano* **2017**, *11*, 12008.
[3] A. Ivanova, B. Frka-Petesic, A. Paul, T. Wagner, A. N. Jumabekov, Y. Vilk, J. Weber, J. S. A. D. Günne, S. Vignolini, M. Tiemann, D. Fattakhova-Rohlfing, T. Bein, *ACS Appl. Mater. Interfaces* **2020**, *12*, 12639.
[4] A. Espinha, G. Guidetti, M. C. Serrano, B. Frka-Petesic, A. G. Dumanli, W. Y. Hamad, Á. Blanco, C. López, S. Vignolini, *ACS Appl. Mater. Interfaces* **2016**, *8*, 31935.
[5] C. E. Boott, A. Tran, W. Y. Hamad, M. J. MacLachlan, *Angew. Chem.* **2020**, *132*, 232.
[6] J.-F. Revol, D. L. Godbout, D. G. Gray, *J. Pulp Pap. Sci.* **1998**, *24*, 146.
[7] J. P. F. Lagerwall, C. Schütz, M. Salajkova, J. Noh, J. H. Park, G. Scalia, L. Bergström, *NPG Asia Mater* **2014**, *6*, e80.
[8] R. M. Parker, G. Guidetti, C. A. Williams, T. Zhao, A. Narkevicius, S. Vignolini, B. Frka-Petesic, *Adv. Mater.* **2018**, *30*, 1704477.
[9] C. Schütz, J. R. Bruckner, C. Honorato-Rios, Z. Tosheva, M. Anyfantakis, J. P. F. Lagerwall, *Crystals* **2020**, *10*, 199.
[10] M. S. Reid, M. Villalobos, E. D. Cranston, *Langmuir* **2017**, *33*, 1583.
[11] R. S. Reiner, A. W. Rudie, in *Production and Applications of Cellulose Nanomaterials* (Eds: M. T. Postek, R. J. Moon, A. W. Rudie, M. A. Bilodeau), TAPPI Press, Peachtree Corners, GA **2013**, pp. 21–24.
[12] J. Miller, *2018-September- Cellulose Nanomaterials Production Summary, TAPPI*, **2018**, https://www.tappinano.org/media/1266/2018-cellulose-nanomaterials-production-update.pdf.
[13] J.-F. F. Revol, H. Bradford, J. Giasson, R. H. H. Marchessault, D. G. G. Gray, *Int. J. Biol. Macromol.* **1992**, *14*, 170.
[14] J.-F. Revol, L. Godbout, X.-M. Dong, D. G. Gray, H. Chanzy, G. Maret, *Liq. Cryst.* **1994**, *16*, 127.
[15] H. de Vries, *Acta Crystallogr.* **1951**, *4*, 219.
[16] R. Bardet, F. Roussel, S. Coindeau, N. Belgacem, J. Bras, *Carbohydr. Polym.* **2015**, *122*, 367.

[17] M. K. Khan, A. Bsoul, K. Walus, W. Y. Hamad, M. J. Maclachlan, *Angew. Chem., Int. Ed.* **2015**, *54*, 4304.
[18] T. H. Zhao, R. M. Parker, C. A. Williams, K. T. P. Lim, B. Frka-Petesic, S. Vignolini, *Adv. Funct. Mater.* **2019**, *29*, 1804531.
[19] K. Yao, Q. Meng, V. Bulone, Q. Zhou, *Adv. Mater.* **2017**, *29*, 1701323.
[20] R. Bardet, N. Belgacem, J. Bras, *ACS Appl. Mater. Interfaces* **2015**, *7*, 4010.
[21] A. Querejeta-Fernández, B. Kopera, K. S. Prado, A. Klinkova, M. Methot, G. Chauve, J. Bouchard, A. S. Helmy, E. Kumacheva, *ACS Nano* **2015**, *9*, 10377.
[22] M. G. Campbell, Q. Liu, A. Sanders, J. S. Evans, I. I. Smalyukh, *Materials* **2014**, *7*, 3021.
[23] K. E. Shopsowitz, H. Qi, W. Y. Hamad, M. J. MacLachlan, *Nature* **2010**, *468*, 422.
[24] K. E. Shopsowitz, W. Y. Hamad, M. J. MacLachlan, *J. Am. Chem. Soc.* **2012**, *134*, 867.
[25] X. Mu, D. G. Gray, *Langmuir* **2014**, *30*, 9256.
[26] G. Guidetti, S. Atifi, S. Vignolini, W. Y. Hamad, *Adv. Mater.* **2016**, *28*, 10042.
[27] D. V. Saraiva, R. Chagas, B. M. de Abreu, C. N. Gouveia, P. E. S. Silva, M. H. Godinho, S. N. Fernandes, *Crystals* **2020**, *10*, 122.
[28] B. Zhu, R. Merindol, A. J. Benitez, B. Wang, A. Walther, *ACS Appl. Mater. Interfaces* **2016**, *8*, 11031.
[29] M. Gu, C. Jiang, D. Liu, N. Prempeh, I. I. Smalyukh, *ACS Appl. Mater. Interfaces* **2016**, *8*, 32565.
[30] C. M. Walters, C. E. Boott, T. D. Nguyen, W. Y. Hamad, M. J. Maclachlan, *Biomacromolecules* **2020**, *21*, 1295.
[31] H. Thérien-Aubin, A. Lukach, N. Pitch, E. Kumacheva, *Angew. Chem., Int. Ed.* **2015**, *54*, 5618.
[32] H. Thérien-Aubin, A. Lukach, N. Pitch, E. Kumacheva, *Angew. Chem.* **2015**, *127*, 5710.
[33] Q. Liu, M. G. Campbell, J. S. Evans, I. I. Smalyukh, *Adv. Mater.* **2014**, *26*, 7178.
[34] Y. Li, E. Prince, S. Cho, A. Salari, Y. Mosaddeghian Golestani, O. D. Lavrentovich, E. Kumacheva, *Proc. Natl. Acad. Sci. U. S. A.* **2017**, *114*, 2137.
[35] A. C. Trindade, M. Carreto, G. Helgesen, K. D. Knudsen, F. Puchtler, J. Breu, S. Fernandes, M. H. Godinho, J. O. Fossum, *Eur. Phys. J.: Spec. Top.* **2020**, *229*, 2741.
[36] B. D. Lawrence, M. Cronin-Golomb, I. Georgakoudi, D. L. Kaplan, F. G. Omenetto, *Biomacromolecules* **2008**, *9*, 1214.
[37] Z. Zhou, S. Zhang, Y. Cao, B. Marelli, X. Xia, T. H. Tao, *Adv. Mater.* **2018**, *30*, 1706983.
[38] B. Marelli, M. A. Brenckle, D. L. Kaplan, F. G. Omenetto, *Sci. Rep.* **2016**, *6*, 25263.
[39] L. D. Koh, Y. Cheng, C. P. Teng, Y. W. Khin, X. J. Loh, S. Y. Tee, M. Low, E. Ye, H. D. Yu, Y. W. Zhang, M. Y. Han, *Prog. Polym. Sci.* **2015**, *46*, 86.
[40] H. Sun, B. Marelli, *Nat. Commun.* **2020**, *11*, 351.
[41] H. Perry, A. Gopinath, D. L. Kaplan, L. D. Negro, F. G. Omenetto, *Adv. Mater.* **2008**, *20*, 3070.
[42] S. Kim, A. N. Mitropoulos, J. D. Spitzberg, H. Tao, D. L. Kaplan, F. G. Omenetto, *Nat. Photonics* **2012**, *6*, 818.
[43] G. Guidetti, Y. Wang, F. G. Omenetto, *Nanophotonics* **2020**, *10*, 137.
[44] B. Marelli, N. Patel, T. Duggan, G. Perotto, E. Shirman, C. Li, D. L. Kaplan, F. Omenetto, *Proc. Natl. Acad. Sci. U. S. A.* **2017**, *114*, 451.
[45] M. Zhu, H. Y. Yu, F. Tang, Y. Li, Y. Liu, J.-m. Yao, *Chem. Eng. J.* **2020**, *394*, 124855.
[46] L. Liu, J. M. Yao, *Adv. Mater. Res.* **2011**, *175–176*, 272.
[47] L. Liu, X. Yang, H. Yu, C. Ma, J. Yao, *RSC Adv.* **2014**, *4*, 14304.
[48] G. Freddi, M. Romanò, M. R. Massafra, M. Tsukada, *J. Appl. Polym. Sci.* **1995**, *56*, 1537.
[49] G. Yang, L. Zhang, Y. Liu, *J. Memb. Sci.* **2000**, *177*, 153.
[50] S. Hirano, T. Nakahira, M. Zhang, M. Nakagawa, M. Yoshikawa, T. Midorikawa, *Carbohydr. Polym.* **2002**, *47*, 121.
[51] L. Zhou, Q. Wang, J. Wen, X. Chen, Z. Shao, *Polymer (Guildf)* **2013**, *54*, 5035.
[52] R. Boy, G. Narayanan, R. Kotek, in *Polysaccharide-Based Fibers and Composites: Chemical and Engineering Fundamentals and Industrial Applications*, Springer, Cham **2017**, pp. 77.
[53] Y. Noishiki, Y. Nishiyama, M. Wada, S. Kuga, J. Magoshi, *J. Appl. Polym. Sci.* **2002**, *86*, 3425.
[54] D. J. Park, Y. Choi, S. Heo, S. Y. Cho, H. J. Jin, *J. Nanosci. Nanotechnol.* **2012**, *12*, 6139.
[55] R. Li, Y. Zhang, L. Zhu, J. Yao, *J. Appl. Polym. Sci.* **2012**, *124*, 2080.
[56] J. Huang, L. Liu, J. Yao, *Fibers Polym.* **2011**, *12*, 1002.
[57] P. Dorishetty, R. Balu, S. S. Athukoralalage, T. L. Greaves, J. Mata, L. De Campo, N. Saha, A. C. W. Zannettino, N. K. Dutta, N. R. Choudhury, *ACS Sustainable Chem. Eng.* **2020**, *8*, 2375.
[58] S. Y. Cho, M. E. Lee, Y. Choi, H. J. Jin, *Fibers Polym.* **2014**, *15*, 215.
[59] J. H. Lee, C. H. Bae, B.-D. Park, I. C. Um, *Int. J. Ind. Entomol.* **2013**, *26*, 81.
[60] Y. Feng, X. Li, M. Li, D. Ye, Q. Zhang, R. You, W. Xu, *ACS Sustainable Chem. Eng.* **2017**, *5*, 6227.
[61] C. Narita, Y. Okahisa, K. Yamada, *J. Clean. Prod.* **2019**, *234*, 200.
[62] A. G. Dumanli, H. M. van der Kooij, G. Kamita, E. Reisner, J. J. Baumberg, U. Steiner, S. Vignolini, *ACS Appl. Mater. Interfaces* **2014**, *6*, 12302.
[63] G. Perotto, Y. Zhang, D. Naskar, N. Patel, D. L. Kaplan, S. C. Kundu, F. G. Omenetto, *Appl. Phys. Lett.* **2017**, *111*, 103702.
[64] G. Singh, C. Chandoha-Lee, W. Zhang, S. Renneckar, P. J. Vikesland, A. Pruden, *Water Res.* **2016**, *104*, 137.
[65] Y. Cao, B. Wang, *Int. J. Mol. Sci.* **2009**, *10*, 1514.
[66] *Canada Gaz. Part II (Order 2012-87-09-01 Amend. Domest. Subst. List.* **2012**, *146*, 2452.
[67] H. Tao, M. A. Brenckle, M. Yang, J. Zhang, M. Liu, S. M. Siebert, R. D. Averitt, M. S. Mannoor, M. C. McAlpine, J. A. Rogers, D. L. Kaplan, F. G. Omenetto, *Adv. Mater.* **2012**, *24*, 1067.
[68] E. Fortunati, M. Peltzer, I. Armentano, L. Torre, A. Jiménez, J. M. Kenny, *Carbohydr. Polym.* **2012**, *90*, 948.
[69] B. Frka-Petesic, G. Kamita, G. Guidetti, S. Vignolini, *Phys. Rev. Mater.* **2019**, *3*, 045601.
[70] B. Frka-Petesic, G. Guidetti, G. Kamita, S. Vignolini, *Adv. Mater.* **2017**, *29*, 1701469.
[71] B. Frka-Petesic, J. A. Kelly, G. Jacucci, G. Guidetti, G. Kamita, N. P. Crossette, W. Y. Hamad, M. J. MacLachlan, S. Vignolini, *Adv. Mater.* **2020**, *32*, 1906889.
[72] Y. Bouligand, *Tissue Cell* **1972**, *4*, 189.
[73] J. Majoinen, E. Kontturi, O. Ikkala, D. G. Gray, *Cellulose* **2012**, *19*, 1599.
[74] J. G. Hardy, L. M. Römer, T. R. Scheibel, *Polymer (Guildf)* **2008**, *49*, 4309.
[75] S. Y. Oh, I. Y. Dong, Y. Shin, C. K. Hwan, Y. K. Hak, S. C. Yong, H. P. Won, H. Y. Ji, *Carbohydr. Res.* **2005**, *340*, 2376.
[76] Y. Liu, H. Hu, *Fibers Polym.* **2008**, *9*, 735.
[77] Y. Yue, C. Zhou, A. D. French, G. Xia, G. Han, Q. Wang, Q. Wu, *Cellulose* **2012**, *19*, 1173.
[78] H. Zhang, L. ling Li, F. yin Dai, H. hao Zhang, B. Ni, W. Zhou, X. Yang, Y. zhang Wu, *J. Transl. Med.* **2012**, *10*, 117.
[79] M. Fan, D. Dai, B. Huang, in *Fourier Transform – Materials Analysis* (Ed: S. Salih), InTech, China **2012**, pp. 1.
[80] C. F. Liu, R. C. Sun, A. P. Zhang, J. L. Ren, Z. C. Geng, *Polym. Degrad. Stab.* **2006**, *91*, 3040.
[81] X. Hu, D. Kaplan, P. Cebe, *Macromolecules* **2006**, *39*, 6161.
[82] A. Matsumoto, J. Chen, A. L. Collette, U. J. Kim, G. H. Altman, P. Cebe, D. L. Kaplan, *J. Phys. Chem. B* **2006**, *110*, 21630.

[83] J. Magoshi, M. Mizuide, T. Magoshi, K. Takahashi, M. Kubo, S. Nakamura, *J. Polym. Sci., Polym. Phys. Ed.* **1979**, *17*, 515.
[84] D. M. Byler, H. Susi, *Biopolymers* **1986**, *25*, 469.
[85] S. Inoue, K. Tanaka, F. Arisaka, S. Kimura, K. Ohtomo, S. Mizuno, *J. Biol. Chem.* **2000**, *275*, 40517.
[86] C. W. P. Foo, E. Bini, J. Hensman, D. P. Knight, R. V. Lewis, D. L. Kaplan, *Appl. Phys. A: Mater. Sci. Process.* **2006**, *82*, 223.
[87] H. Y. Wang, Y. Q. Zhang, *Soft Matter* **2013**, *9*, 138.
[88] T. Lu, H. Pan, J. Ma, Y. Li, S. W. Bokhari, X. Jiang, S. Zhu, D. Zhang, *ACS Appl. Mater. Interfaces* **2017**, *9*, 18231.
[89] Z. Zhang, B. Zhang, N. Grishkewich, R. Berry, K. C. Tam, *Adv. Sustainable Syst.* **2019**, *3*, 1800156.
[90] Z. Ling, K. Wang, W. Liu, W. Tang, Q. Yong, *J. Mater. Chem. C* **2020**, *8*, 8493.
[91] D. N. Rockwood, R. C. Preda, T. Yücel, X. Wang, M. L. Lovett, D. L. Kaplan, *Nat. Protoc.* **2011**, *6*, 1612.